Boundary Layer Characteristics over Homogeneous and Heterogeneous Surfaces Simulated by MM5 and DALES

MIRANDA BRAAM, JORDI VILÀ-GUERAU DE ARELLANO, AND MONICA GÓRSKA

Meteorology and Air Quality Section, Wageningen University, Wageningen, Netherlands

(Manuscript received 10 May 2010, in final form 8 December 2010)

ABSTRACT

The multiple-single-column approach is proposed as a new concept to study the boundary layer parameterization scheme in the fifth-generation Pennsylvania State University–National Center for Atmospheric Research Mesoscale Model (MM5). The results are compared with the Dutch Atmospheric Large-Eddy Simulation Model (DALES). Numerical experiments were performed over homogeneous and heterogeneous surfaces under clear convective boundary layer conditions. Identical simulations using MM5 and DALES were performed, which enabled an evaluation of the MM5 boundary layer scheme with DALES results. From the experiment with a homogeneous surface, MM5 shows a slightly shallower, colder, and moister boundary layer than DALES. This result is produced by an underestimation of turbulent mixing near the surface and less-vigorous entrainment of heat and dry air in MM5. In the heterogeneous surface experiment, the domain is divided into dry and wet patches, with the result that both models produce a mesoscale circulation. However, relative to the homogeneous case, larger differences were found between the models in the representation of the boundary layer dynamics. In DALES, the surface heterogeneity influenced the turbulent motions, making the mesoscale circulation much stronger (w_{max} is 6 times as large) than in MM5. Because of this stronger circulation, the boundary layer height, bulk temperature, and humidity also displayed differences in time and spatial patterns. Because of the land–atmosphere coupling in MM5, the mesoscale circulation strengthened the surface flux heterogeneity. Cold and moist air advection close to the surface from the wet patch to the dry patch increased the sensible heat flux above the dry patch and thus the induced mesoscale flow.

1. Introduction

The performance of parameterization schemes (e.g., the boundary layer scheme) in mesoscale models is normally examined by means of observational case studies (Grell et al. 1994; Zhong et al. 2007; Steeneveld et al. 2008). A shortcoming of this method is that it is very difficult to discriminate the effects of land–atmosphere couplings (Ek and Mahrt 1994) in and between the parameterization schemes because of the complexity of a real situation. A more transparent method is to validate the parameterization schemes in single-column models (SCM) against a large-eddy simulation model (LES; Lenderink et al. 2004). Because of the one-dimensionality of an SCM, the model is restricted to the prescribed boundary conditions—namely, large-scale external forcing—and the model has less freedom to adapt internally to variations in these conditions. Closely related to this point is that the influences of horizontal surface variability cannot be studied. We here propose an alternative concept: the mesoscale model is initialized and updated with idealized surface and upper air conditions in every grid box over the entire domain instead of employing the forcing provided by large-scale atmospheric models such as those of the European Centre for Medium-Range Weather Forecasts (ECMWF) or National Centers for Environmental Prediction (NCEP) as is normally used (standard procedure; Grell et al. 1994; Zhong et al. 2007; Steeneveld et al. 2008). Simulating a control run in the mesoscale model enabled us to perform identical numerical experiments over homogeneous and heterogeneous surfaces using the mesoscale model and the LES, which is a three-dimensional model in which turbulence is explicitly calculated. This method will be referred to as the multiple-single-column (MSC) approach. The MSC approach has as an advantage in that by performing control academic simulations in a mesoscale model (instead of using the standard procedure) the method retains the benefits of a SCM.

Corresponding author address: Miranda Braam, Wageningen University, P.O. Box 47, 6700 AA Wageningen, Netherlands.
E-mail: miranda.braam@wur.nl

DOI: 10.1175/2011JAMC2552.1

Another benefit is that the MSC technique can be used to investigate the influence of horizontal surface variability on atmospheric phenomena, because we are able to design experiments with a domain consisting of multiple grid cells interacting with each other. In this study we compare the Medium Range Forecast (MRF) boundary layer scheme (Hong and Pan 1996) from version 3.6.1 of the nonhydrostatic fifth-generation Pennsylvania State University–National Center for Atmospheric Research Mesoscale Model (MM5; Grell et al. 1994) with the Dutch Atmospheric Large-Eddy Simulation Model (DALES; Heus et al. 2010). To this end, we have performed a series of idealized numerical control experiments with the same surface forcing as in DALES using the MSC technique applied to MM5. From the results of the experiments, we determine the role of homogeneous and heterogeneous surface forcing in boundary layer development.

The first idealized experiment (the homogeneous surface case) was designed to answer the following question: How are the boundary layer dynamics (e.g., vertical structure of temperature, humidity and turbulent fluxes, boundary layer height, and entrainment processes) represented by the MRF boundary layer scheme, which is a first-order nonlocal scheme (Troen and Mahrt 1986; Holtslag and Boville 1993), in comparison with DALES in which turbulence is explicitly calculated? We selected the MRF scheme because it is specially designed for the convective boundary layer and has been shown to simulate the daytime boundary layer structures more realistically than do other available schemes (Holtslag et al. 1995; Hong and Pan 1996; Vilà-Guerau de Arellano et al. 2001; Zhong and Fast 2003). To investigate the sensitivity to entrainment under homogeneous surface conditions, the results obtained by MM5 and DALES were compared with data from a mixed-layer model (MXL; Tennekes and Driedonks 1981). We use MXL because it has an explicit representation of entrainment, which gives us an additional quantification of the role of the entrainment in the heat and moisture budget.

A limitation of boundary layer schemes is that the majority of them are designed for and tested under homogeneous horizontal conditions. To investigate their performance over a heterogeneous land surface, we simulated a second control experiment, involving two patches with a difference in soil moisture availability. Land surface heterogeneity in soil moisture is of interest because it has a direct effect on the surface heat fluxes. In turn, it influences the evolution of boundary layer dynamics (e.g., boundary layer depth and the structure of temperature and humidity within the boundary layer) and it generates mesoscale circulations driven by the thermal forcing differences. The influences on boundary layer dynamics and on the formation of mesoscale circulations depend on a number of variables, including the heterogeneity length scale, amplitude differences in the surface flux heterogeneity, and the geostrophic wind (Avissar and Schmidt 1998; Mahrt 2000).

TABLE 1. The parameterization schemes used in the homogeneous and heterogeneous MM5 experiments.

	Domains 1 (837×837 km^2) and 2 (279×279 km^2)	Domains 3 (93×93 km^2) and 4 (31×31 km^2)
Cumulus	Kain–Fritsch	None
Moisture	Simple ice	Simple ice
PBL	Medium-range forecast	Medium-range forecast
Radiation	Simple cooling	Simple cooling
Surface	Five-layer soil model	Five-layer soil model

Several theoretical studies have investigated modifications of boundary layer characteristics by surface heterogeneity (Avissar and Schmidt 1998; Patton et al. 2005; Letzel and Raasch 2003; van Heerwaarden and Vilà-Guerau de Arellano 2008). Focusing, for instance, on the heterogeneity length scale, Avissar and Schmidt (1998) found from a numerical experiment with LES that the length scales of patches smaller than 5–10 km had hardly any influence on boundary layer dynamics, whereas larger heterogeneous patches did. Patton et al. (2005) observed that the most intense patch-induced motion occurs when the length scale divided by the boundary layer height was between 4 and 9.

Observational studies have also shown the influence of surface heterogeneity on boundary layer dynamics. By analyzing the surface and aircraft measurements of the 2002 International H_2O Project (IHOP_2002; Weckwerth et al. 2004), LeMone et al. (2007) determined the impact of nonuniform grass and wheat vegetation and the season on the surface heat fluxes.

Our study extended these previous studies by analyzing a heterogeneous control experiment using MM5 and DALES. The heterogeneous case was inspired by data from IHOP_2002. It was characterized by a dry patch and a wet patch, each with a width of 15 km, which is larger than the critical scale as mentioned by Avissar and Schmidt (1998) and Patton et al. (2005). In brief, the study under heterogeneous conditions asked two main questions: 1) How is the induced mesoscale circulation represented by MM5, as compared with DALES? 2) Are the modeled surface fluxes in MM5 influenced by the induced mesoscale circulation (atmosphere–land interactions)? To the best of our knowledge, this is the first time that a mesoscale model and an LES have been compared using control numerical simulations with identical surface forcing.

TABLE 2. Surface characteristics employed in the homogeneous and heterogeneous MM5 experiments.

	Soil moisture (%)	Albedo (%)	Emissivity at 9 mm (%)	Roughness length (cm)	Thermal inertia (cal cm^{-2} K^{-1} $s^{-1/2}$)	Soil heat capacity (J K^{-1} m^{-3})
Homogeneous	50	19	92	12	3	0.60
Heterogeneous	30 (west)	19	92	12	3	0.60
	70 (east)	19	92	12	3	0.60

The paper is structured as follows. The models under study are described in section 2. In section 3, we examine first the homogeneous case, including the discussion of temperature and humidity profiles, boundary layer height, and the role of entrainment. We then study the heterogeneous case: the induced circulation characteristics and boundary layer structure above the two patches. The influences of the atmosphere–land interactions on the fluxes from MM5 are shown and quantified in section 3c. Our conclusions are drawn in the final section.

2. Model description and research strategy

a. MM5

MM5 used four one-way nested domains of 31 by 31 grid points with grid lengths of 27, 9, 3, and 1 km, respectively. All of the domains shared a central point at 37.40°N, 96.73°W; consequently this was a midlatitude numerical experiment with a Coriolis force of $f = 8.9 \times 10^{-5}$ s^{-1}. There were 39 vertical sigma levels. To ensure that the vertical resolution in the boundary layer was sufficiently detailed, 20 sigma levels were defined in the lowest 1500 m, which correspond to a resolution of 50–100 m. All the domains were run without spinup time from 0700 local time (LT) 30 May until 0100 LT 31 May.

The physical parameterization schemes used in the numerical MM5 experiments are shown in Table 1. The MRF scheme is a first-order nonlocal scheme based on Troen and Mahrt (1986) and Holtslag and Boville (1993). The turbulent fluxes of potential temperature ($\overline{w'\theta'}$) and specific humidity ($\overline{w'q'}$) are calculated as follows:

$$\overline{w'\theta'} = -K_h\left(\frac{\partial\overline{\theta}}{\partial z} - \gamma_h\right) \quad \text{and} \tag{1}$$

$$\overline{w'q'} = -K_q\left(\frac{\partial\overline{q}}{\partial z} - \gamma_q\right), \tag{2}$$

in which $K_{h,q}$ is the exchange coefficient [$K_{h,q} = K_m\text{Pr}^{-1} = kw_sz(1 - z/h)^2\text{Pr}^{-1}$, in which Pr is the turbulent Prandtl number, k is the von Kármán constant, w_s is the convective boundary layer velocity scale, and h is the boundary layer height], $\gamma_{h,q}$ is the countergradient for heat (subscript h) and moisture (subscript q), and $\partial\theta/\partial z$ and $\partial q/\partial z$ are the gradients of potential temperature θ and specific humidity q, respectively. MRF first calculates h using the parcel method estimated as

$$h = \frac{\text{Ri}_{\text{cr}}T_0|V(h)|^2}{g[\theta_v(h) - \theta_s]},$$

in which RI_{cr} is the critical Richardson number, $V(h)$ and $\theta_v(h)$ are the horizontal wind speed and virtual potential temperature at level h, g is the acceleration of gravity, and θ_s is the surface temperature [see Fig. 2 of Holtslag and Boville (1993) for an illustrative figure of the parcel method]. Note that by using these equations, entrainment is not explicitly parameterized in MRF.

By connecting MRF with the five-layer soil surface scheme, the surface sensible heat flux H and latent heat flux L_vE are obtained with the following equations:

$$H = \rho c_p C_h u_*(\theta_s - \theta_a) \quad \text{and} \tag{3}$$

$$L_vE = \rho L_v M C_q u_*(q_s - q_a), \tag{4}$$

in which ρ is the air density, c_p is the specific heat, L_v is the latent heat, M is the soil moisture availability, $C_{h,q}$ is the surface drag coefficient for heat (subscript h) and moisture (subscript q), u_* is the friction velocity, and $\theta_s - \theta_a$ and $q_s - q_a$ are the differences between the surface and the first atmospheric level for potential temperature and specific humidity, respectively.

As mentioned above, we modified the surface and upper-air conditions over the entire domain to perform idealized numerical experiments (MSC approach). The following conditions were prescribed at the surface: 1) terrain height was set to 0 m over the total area, 2) surface pressure was 1010 hPa for every grid point, 3) land use—namely, grassland—was set to be the same for every grid point based on the U.S. Geological Survey table, and 4) the land mask of a few grid points was changed from water to land, leaving the entire domain as uniform land. The corresponding surface characteristics are shown in Table 2.

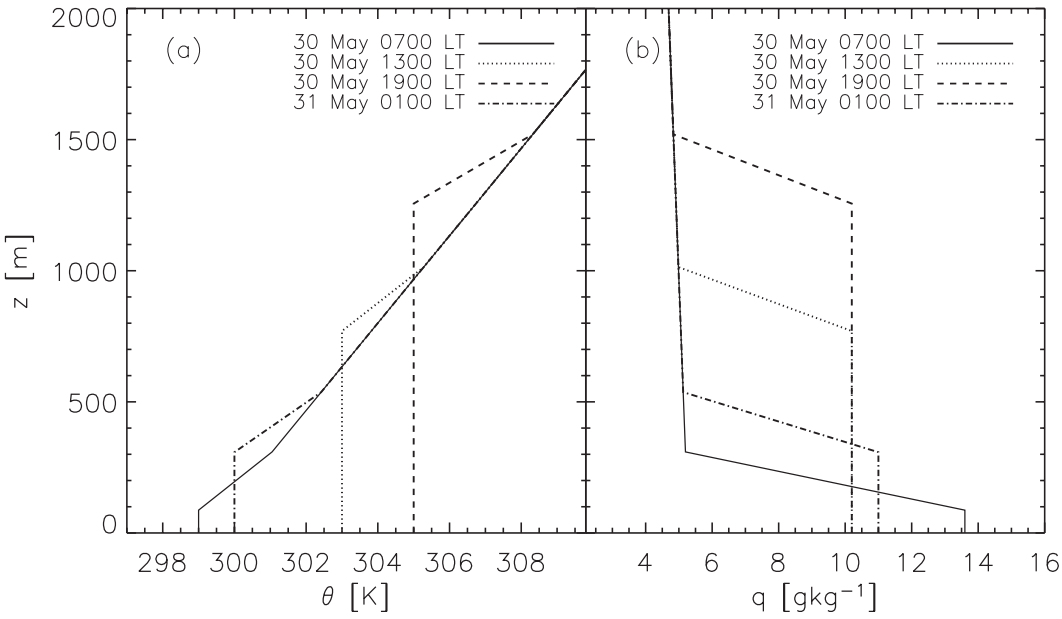

FIG. 1. The initial and boundary condition profiles of (a) potential temperature and (b) specific humidity at 0700 (solid lines), 1300 (dotted lines), and 1900 (dashed lines) LT 30 May and 0100 (dot–dashed lines) LT 31 May 2002.

We performed two numerical MM5 experiments, one using homogeneous surface conditions and one using heterogeneous surface conditions. The former had a soil moisture availability of 50% across the entire domain. To ascertain whether this MM5 control experiment showed uniform surface forcing over the entire domain, we determined the relative standard deviation [$\mathrm{RSD}_x = (\sigma_x/\overline{x}) \times 100\%$; in our case, σ_x is the horizontal spatial standard deviation and $\overline{x}$ is the horizontal spatial mean] of H and L_vE. RSD_H over the fourth domain was around 10% during the morning and evening transition periods (when $\overline{H}$ is small) and was below 1% during unstable conditions. For L_vE the relative standard deviation throughout the day was very low—below 0.01%. These observations indicated that surface forcing was homogeneous.

For the heterogeneous case, the area was divided into two patches. The western patch (with a width of 15 grid boxes) had smaller values for soil moisture ($M = 30\%$) than the eastern patch (16 grid boxes; $M = 70\%$). This produced larger values for the sensible heat fluxes in the west also observed during IHOP_2002 (LeMone et al. 2007; Górska et al. 2008). The soil moisture heterogeneity was only applied to the smallest domain, because the horizontal scale (31×31 km^2) was comparable to the horizontal scale of the DALES experiment (25.6×25.6 km^2). The heterogeneous length scales λ were thus 15.5 and 12.8 km for MM5 and DALES, respectively.

In mesoscale models, the upper-air conditions of the first domain are usually obtained from global weather forecasts such as ECMWF or NCEP. MM5 needs an update for the temperature, wind speed, and relative humidity three-dimensional fields. In our study, we adopted a different approach (MSC); to obtain a fully idealized control experiment, the upper-air conditions were explicitly prescribed for every grid point every 6 h. The new prescribed conditions were inspired by observations from IHOP_2002 (Górska et al. 2008) and are provided in Fig. 1 and Table 3. Note that the background geostrophic wind is small. The experiments are thus close to free-convection conditions. By using the MSC approach instead of the standard procedure of MM5, the method has the benefits inherent to SCM, and next to that the effect of surface heterogeneity can be investigated as well.

To consider surface variability, we treated the MM5 three-dimensional fields as follows: in the homogeneous case, data of the smallest domain were analyzed by averaging over the entire domain to improve the statistical robustness of our results relative to the usual single gridpoint comparisons. In the heterogeneous case, we utilized three different methods of spatial data averaging: 1) over the entire smallest domain as in the homogeneous case, 2) over the west and east patches separately, to investigate the differences between the two patches, and 3) over the latitude for every degree of longitude, to study the variability along the surface heterogeneity. Furthermore, the MM5 output was saved every hour.

b. *Large-eddy simulation*

DALES (Heus et al. 2010) solves the filtered thermodynamic equations. It thus calculates explicitly the

TABLE 3. Initial and boundary conditions employed in the homogeneous and heterogeneous MM5 experiments: the boundary layer values (bl), the jump at the inversion (Δ), and the gradient in the free atmosphere (γ) for the potential temperature θ and specific humidity q; boundary layer height z_{bl}; and the wind speed in the east–west and south–north directions (U and V, respectively).

	0700 LT 30 May (t = 0 h)	1300 LT 30 May (t = 6 h)	1900 LT 30 May (t = 12 h)	0100 LT 31 May (t = 18 h)
θ_{bl} (K)	299	303	305	300
$\Delta\theta$ (K)	2	2.2	2.6	2.2
γ_θ (K m^{-1})	6×10^{-3}	6×10^{-3}	6×10^{-3}	6×10^{-3}
q_{bl} (g kg^{-1})	13.6	10.2	10.2	11
Δq (g kg^{-1})	−8.4	−5.21	−5.33	−5.86
γ_q (g kg^{-1} m^{-1})	-3×10^{-4}	-3×10^{-4}	-3×10^{-4}	-3×10^{-4}
z_{bl} (m)	300	1000	1400	500
U (m s^{-1})	0	0	0	0
V (m s^{-1})	1	1	1	1

most energetic turbulent eddy motions (between 80% and 90% are resolved without parameterization) in the convective boundary layer. The subgrid motions are parameterized with the eddy diffusivity coefficient and the local gradients. The surface heat fluxes in DALES are prescribed. The domain was $25.6 \times 25.6 \times 2.7$ km^3 with a grid box of $100 \times 100 \times 25$ m^3. The central point is located at 37.40°N, 96.73°W as in MM5. The simulation ran for 12 h, starting at 0700 LT. The initial conditions of θ and q were the same as those of MM5 (see solid line in Fig. 1 and the first column of Table 3). To spin up the laminar flow in the boundary layer, subgrid turbulent kinetic energy (TKE) of 2 m^2 s^{-2} in the lowest 300 m was prescribed in DALES.

Homogeneous and heterogeneous cases were simulated, using equal surface conditions as in the mesoscale numerical experiments. Because our LES model did not incorporate land–atmosphere coupling, the daily evolution of surface sensible heat flux H and latent heat flux L_vE had to be prescribed. To simulate the same surface forcing as in MM5, we used the fluxes obtained from the MM5 experiments to prescribe the fluxes in DALES. Since DALES needs to be updated more frequently than every hour, the fluxes in DALES are prescribed with sinusoidal functions in time fitted through the output data of MM5. For the homogeneous run the fluxes were the same over the entire area, whereas in the heterogeneous case different functions were used for the east and west patches (see Table 4 for the functions).

c. Mixed layer model

To complete our study, we employed MXL to determine the sensitivity of our results to entrainment. MXL is a relatively simple conceptual model, in which the entrainment fluxes are explicitly parameterized. In brief, the heat entrainment is based on the zero-order jump approach (Tennekes and Driedonks 1981), which represents the inversion layer as a discontinuity (inversion layer depth is zero). The surface flux $(\overline{w'\theta'_v})_s$ is prescribed and the entrainment flux $(\overline{w'\theta'_v})_e$ is related as follows:

$$(\overline{w'\theta'_v})_e = -\beta_{\theta_v}(\overline{w'\theta'_v})_s.$$

The initial conditions of the MXL run were equal to those of MM5 and DALES. Notice that we used the virtual potential temperature instead of the potential temperature as the mixed-layer variable (see Table 5). Two numerical experiments were performed, using two different ratios of β_{θ_v}. In the first run, a β_{θ_v} of 0.2 (Tennekes 1973) was used. This value has a theoretical background for free-convection situations; some observations and LES studies evidenced higher values, however, which may have been a result of shear at the surface and in the entrainment zone (Pino et al. 2006). To study the sensitivity of this closure value, in our second MXL experiment we specified $\beta_{\theta_v} = 0.4$.

3. Results and discussion

a. Homogeneous case

1) THERMODYNAMIC STRUCTURE AND BOUNDARY LAYER EVOLUTION

In this section the thermodynamic structure of the boundary layer above the homogeneous surface is compared between the two models. Since surface forcing was the same in both models, our preliminary explanations for possible differences are two. First, as explained in section 2a, the MRF scheme is a nonlocal turbulent scheme, in which the boundary layer height is determined using the parcel method. Second, in MRF the representation of entrainment processes is not explicitly calculated as in DALES or explicitly parameterized as in MXL.

Figure 2 shows the potential temperature θ and specific humidity q vertical profiles of MM5 and DALES at 1000, 1300, and 1600 LT. At 1000 LT the potential temperature

TABLE 4. The prescribed surface sensible heat flux ($\overline{w'T'}$; K m s $^{-1}$) and latent heat flux ($\overline{w'q'}$; g kg^{-1} m s^{-1}) for DALES. Here, t is the time in seconds.

	$\overline{w'T'}$	$\overline{w'q'}$
Homogeneous	$0.0568 \times \sin(1.42 \times 10^{-4}t + 1.171) + 0.0542$	$0.1014 \times \sin(1.00 \times 10^{-4}t + 2.869) + 0.0717$
Heterogeneous west: warm and dry patch	$0.1045 \times \sin(1.27 \times 10^{-4}t + 1.745) + 0.0960$	$0.0763 \times \sin(1.00 \times 10^{-4}t + 2.859) + 0.0545$
Heterogeneous east: cold and wet patch	$0.0321 \times \sin(1.52 \times 10^{-4}t + 0.915) + 0.0239$	$0.1205 \times \sin(0.97 \times 10^{-4}t + 3.072) + 0.0789$

in the boundary layer ($\theta_{\rm bl}$) of MM5 and DALES was similar, approximately 300.6 K. During the day, the boundary layer in DALES warmed up more than in MM5. The temperature difference ($\Delta\theta_{\rm DALES-MM5}$) in the middle of the boundary layer (500 m) increased from 0.3 K at 1300 LT to 0.8 K at 1600 LT. Moreover, it was found that the boundary layer of MM5 was deeper in the morning and shallower in afternoon (see also Fig. 3). Another important difference is that θ_s was large in comparison with $\theta_{\rm bl}$ in MM5. The large gradient near the surface shows that MM5 represented less turbulent mixing at the surface than did DALES. A higher vertical resolution may have enhanced the turbulent mixing. The potential benefit of using higher vertical resolution has the disadvantage of defining thin vertical grid cells that could create numerical instabilities, however. Moreover, our aim was to evaluate the scheme under conditions that are similar to those used in mesoscale studies. The difference in the surface gradient may be the reason for the difference in the modeled boundary layer height. In MRF the boundary layer height was calculated as the height at which an air parcel from the surface intersects with the environment temperature profile [see section 2a and Holtslag and Boville (1993)]. In the morning period the high θ_s caused surface parcels to move to higher levels and therefore produced a larger h in MM5. In the afternoon $\theta_{s\rm MM5}$ was lower than $\theta_{\rm blDALES}$. As a result, using the parcel method in MM5 led to a lower h in MM5 than in DALES.

The specific humidity differed between the two models. At 1000 LT, the boundary layer in DALES was wetter than in MM5: $\Delta q_{\rm DALES-MM5} = 0.2$ g kg^{-1}. After 1100 LT, this switched and the boundary layer in MM5 became wetter than in DALES. At 1300 LT we observed $\Delta q_{\rm DALES-MM5} = -0.2$ g kg^{-1} that then rose to -0.5 g kg^{-1} at 1600 LT, with both observations being made at around 500 m. Since surface forcing was the same, the increase in the difference in humidity between DALES and MM5 was related to a greater amount of dry-air entrainment in DALES.

Closely related to the thermodynamic structure is the evolution of the boundary layer height h. From the θ_v profiles, we calculated h according to the gradient method (Sullivan et al. 1998) for MM5 and DALES. Here, h is defined as the location of the maximum virtual potential temperature gradient. MXL calculates h using the entrainment velocity w_e:

$$\frac{\partial h}{\partial t} = w_e = \frac{-(\overline{w'\theta'_v})_e}{\Delta\theta_v},$$

in which $\partial h/\partial t$ is the time derivative of the boundary layer height, $(\overline{w'\theta'_v})_e$ is the entrainment flux, and $\Delta\theta_v$ is the virtual potential temperature jump at the inversion between the atmospheric boundary layer and the free atmosphere. Note that in MM5 and LES the minimum heat flux is observed at a lower level than the maximum potential temperature gradient (Sullivan et al. 1998; Pino et al. 2006), whereas the two levels are located at the same height in MXL because of its physical assumptions.

The boundary layer height evolution calculated from MM5, DALES, and MXL is presented in Fig. 3. As a reference, h as observed by aircraft measurements during IHOP_2002 is included (Górska et al. 2008). The shaded area in Fig. 3 shows h calculated in MXL with β_{θ_v} varying between 0.2 (lower boundary) and 0.4 (upper boundary). We can see that there was a reasonable agreement of the h evolution among all models and observations. The boundary layer height in DALES was smoother than in MM5 because of the greater vertical and temporal resolution of the former.

In comparing DALES and MM5 results, two periods were distinguished: the morning period before 1300 LT

TABLE 5. The prescribed variables for MXL: the mixed layer values (ml), the jump at the inversion (Δ), and the gradient in the free atmosphere (γ) for the virtual potential temperature θ_v, the boundary layer height $z_{\rm bl}$, and the surface buoyancy flux ($\overline{w'T'_v}$; K m s $^{-1}$). Again, t is the time in seconds.

$\theta_{v\rm ml}$ (K)	301.5
$\Delta\theta_v$ (K)	0.47
$\gamma_{\theta v}$ (K m^{-1})	6×10^{-3}
$z_{\rm bl}$ (m)	350
$\overline{w'T'_v}$ (K m s^{-1})	$0.0728 \times \sin(1.37 \times 10^{-4}t + 1.337) + 0.0729$

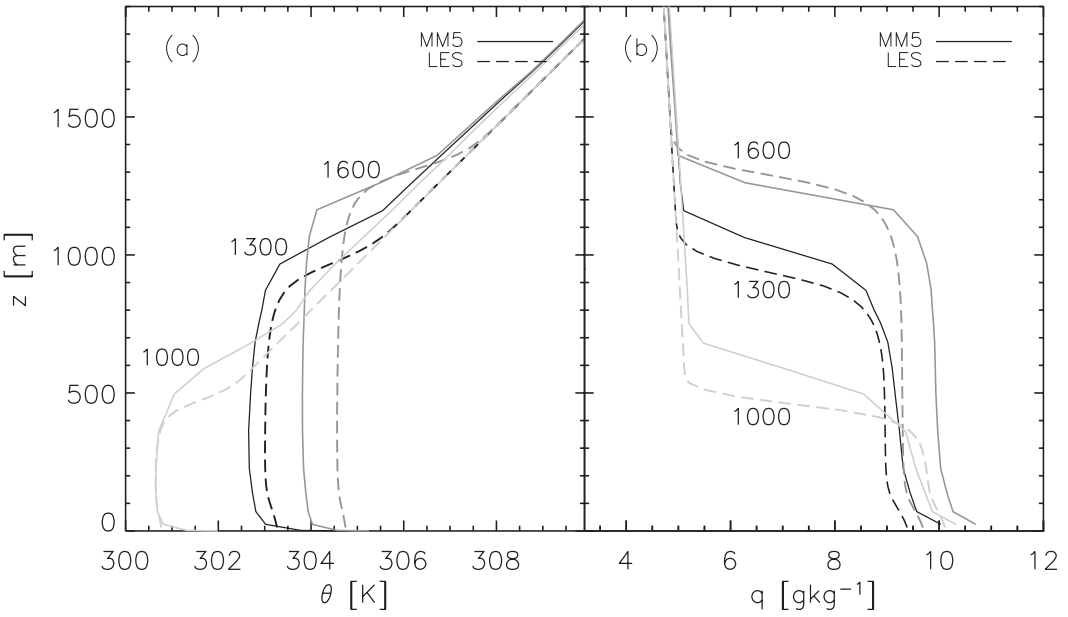

FIG. 2. The vertical profiles of (a) potential temperature and (b) specific humidity at 1000 LT (light-gray lines), 1300 LT (black lines), and 1600 LT (dark-gray lines) from MM5 (solid lines) and DALES (dashed lines). The MM5 vertical profiles (homogeneous case) were averaged over the fourth domain (31×31 km^2), and the DALES profiles were averaged over the 25.6×25.6 km^2 domain.

and the afternoon one after 1400 LT. In the morning the boundary layer was deeper in MM5, whereas h_{DALES} became larger in the afternoon. As explained above, the differences in the boundary layer growth were mainly caused by the combination of the strong θ gradient near the surface and the parcel method in MRF to determine h. However, h is also dependent on entrainment processes. We therefore compared h of MM5 and DALES with the two MXL runs (entrainment parameterized). In the morning, h_{MM5} was located above the shaded area, whereas after 1400 LT it was situated in the lowest part of the area. These observations indicate that in MM5 entrainment processes made a larger contribution to the heat budget in the morning, which decreased in the afternoon. In the course of the day, h_{DALES} was usually located in the upper region of the shaded area, which implies first that entrainment processes are an important contribution to the boundary layer development and second that they require being parameterized explicitly to ensure a proper physical representation. Furthermore it can be mentioned that RSD_h was low for MM5—namely, generally below 1% during unstable conditions—which indicates that the boundary layer height was uniform over the entire domain.

2) Entrainment process representation

To complete the heat and moisture budget in the boundary layer development, we need to quantify the role of entrainment of warm and dry air from the free troposphere. Comparing the results of DALES and MM5 offers us the opportunity to study the differences between the explicitly calculated turbulent fluxes of DALES and the parameterized turbulent fluxes of MM5. The turbulent flux profiles of potential temperature ($\overline{w'\theta'}$) and specific humidity ($\overline{w'q'}$) at 1000 and 1300 LT are shown in Fig. 4. Note that in both models the fluxes do not form part of the output data. In MM5, we subsequently calculated them from the mean gradients of potential temperature and humidity from the three-dimensional fields [Eqs. (1) and (2)]. In DALES, the fluxes were calculated first by using spatial slab averaging and then by time averaging (30 min) following the method of van Heerwaarden and Vilà-Guerau de Arellano (2008). To determine whether DALES can be used as a reference model to validate the parameterization scheme in MM5, the resolved and subgrid contributions of the fluxes are also given. As we show, the turbulent fluxes are mainly resolved in DALES. Only at the lowest 150 m is the subgrid contribution larger than the explicit part. In the entrainment zone the subgrid contribution is relatively low; DALES was consequently used to validate the processes around the entrainment zone modeled by MM5.

The temperature and humidity fluxes calculated from MM5 are in agreement with those calculated from DALES. At specific heights (e.g., for 1000 LT at 50 m

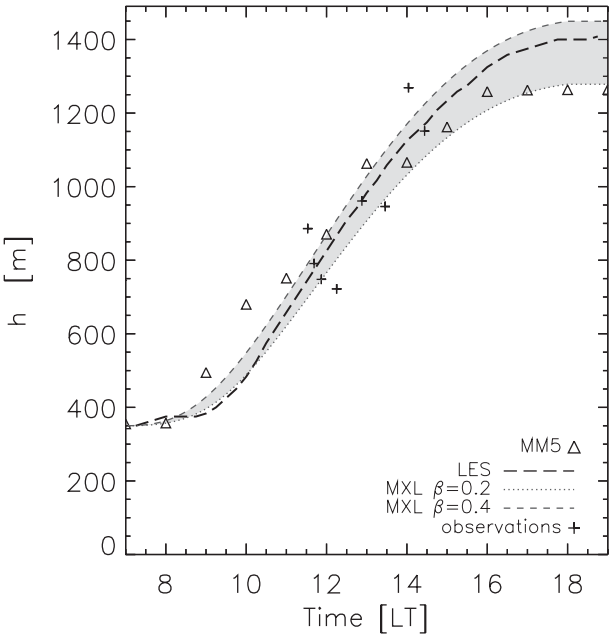

FIG. 3. The evolution of the boundary layer height for the homogeneous case observed from MM5 and DALES. The results of MM5 and DALES were averaged over the entire domain. The shaded region represents the boundary layer height for the mixed layer as calculated with the entrainment velocity taking a zero-order approach with $\beta_{\theta v} = 0.4$ as the upper boundary and $\beta_{\theta v} = 0.2$ as the lower boundary. As a reference, the boundary layer heights from the IHOP_2002 experiment ("observations") are shown.

and for 1300 LT at 200 and 800 m) the flux deviated from that of DALES. Several reasons can be given. First, in MM5, errors in the gradients and therefore in the fluxes can be produced by recalculations of w, θ, and q with rounded output data. Second, the lower vertical resolution in MM5 relative to in DALES can lead to errors.

The linear decrease in $\overline{w'\theta'}$ observed from MM5 was comparable to that found by DALES. Differences were found in the entrainment zone (shaded region in Fig. 4), however. The minimum heat flux in the entrainment zone ($\overline{w'\theta'_e}$) was lower for MM5 than for DALES. It appears that the contrast became greater over the course of the day. At 1000 LT $(\overline{w'\theta'_e})_{\mathrm{DALES}} = -0.032$ K m s^{-1} as compared with $(\overline{w'\theta'_e})_{\mathrm{MM5}} = -0.022$ K m s^{-1}. At 1300 LT the minimum heat flux was -0.042 K m s^{-1} for DALES and -0.022 K m s^{-1} for MM5. At 1700 LT (figure not shown) the entrainment flux of MM5 was very small (-0.007 K m s^{-1}), whereas in DALES we observed -0.034 K m s^{-1}. For the humidity fluxes, MM5 and DALES produced similar patterns. Furthermore, in the entrainment zone the two models again deviated. DALES showed higher values of $\overline{w'q'}$ in the entrainment zone than did MM5. Since the free atmosphere was drier than the boundary layer in this case, the increased entrainment meant that the boundary layer became drier in DALES.

We now quantify in more depth the temporal evolution of entrainment processes in the two models by obtaining an Eulerian flux-portioning method. This method calculated the ratio between N, which is the negative part of the total integral of $\overline{w'\theta'_v}$, and P, which is the positive part ($A = -N/P$). Pino et al. (2006) stated that using this method is more suitable for comparing the entrainment processes of different models than using the value of $(\overline{w'\theta'_v})_e$ because "it takes into account better the regions dominated by the positive heat flux, driven by the surface fluxes and the negative heat flux (entrainment)." In MM5 and DALES, the ratio A is calculated by dividing the negative part (DALES: the gray area in Fig. 4) by the positive part (DALES: below the gray area) of the total integral of the buoyancy flux. For a zero-order model this ratio is defined as $A = \beta^2$; in our MXL this ratio was consequently a fixed constant of 0.04 ($\beta = 0.02$) and 0.16 ($\beta = 0.04$).

Figure 5 shows the diurnal variation in A. Once again, two time periods were distinguished: the morning and the afternoon. First, in the morning, A grew for both models. MM5 underestimated A in comparison with DALES and MXL, however. Since surface forcing was equal in all models, this lower value of A indicates that the entrainment of heat and dry air in MM5 contributed less to their budgets than the other two models did. As a result, during its development the boundary layer will become colder and wetter in MM5. Second, after 1200 LT the ratio observed from DALES remained constant in time at around 0.10 in the middle of the shaded area, indicating that entrainment processes were important for growing, heating, and drying the boundary layer (Fig. 5). The ratio of MM5 fell to values of 0.01. As a result, boundary layer processes were solely driven by surface forcing. This is why in MM5 the boundary layer flattened out in the afternoon and the boundary layer temperature was smaller and the humidity was higher than in DALES.

Summarizing the results of the homogeneous case, we conclude that in MM5 turbulent mixing near the surface and at the entrainment zone is underestimated. Since we had identified the potential limitations of the boundary layer scheme, we then proceeded to determine the impact of surface heterogeneity on the evolution of the boundary layer.

b. Heterogeneous case

1) THE MESOSCALE CIRCULATION

Changes in spatial surface properties induce mesoscale circulations with different strengths. To ascertain both how models simulate a mesoscale circulation and its interaction with the boundary layer dynamics, we

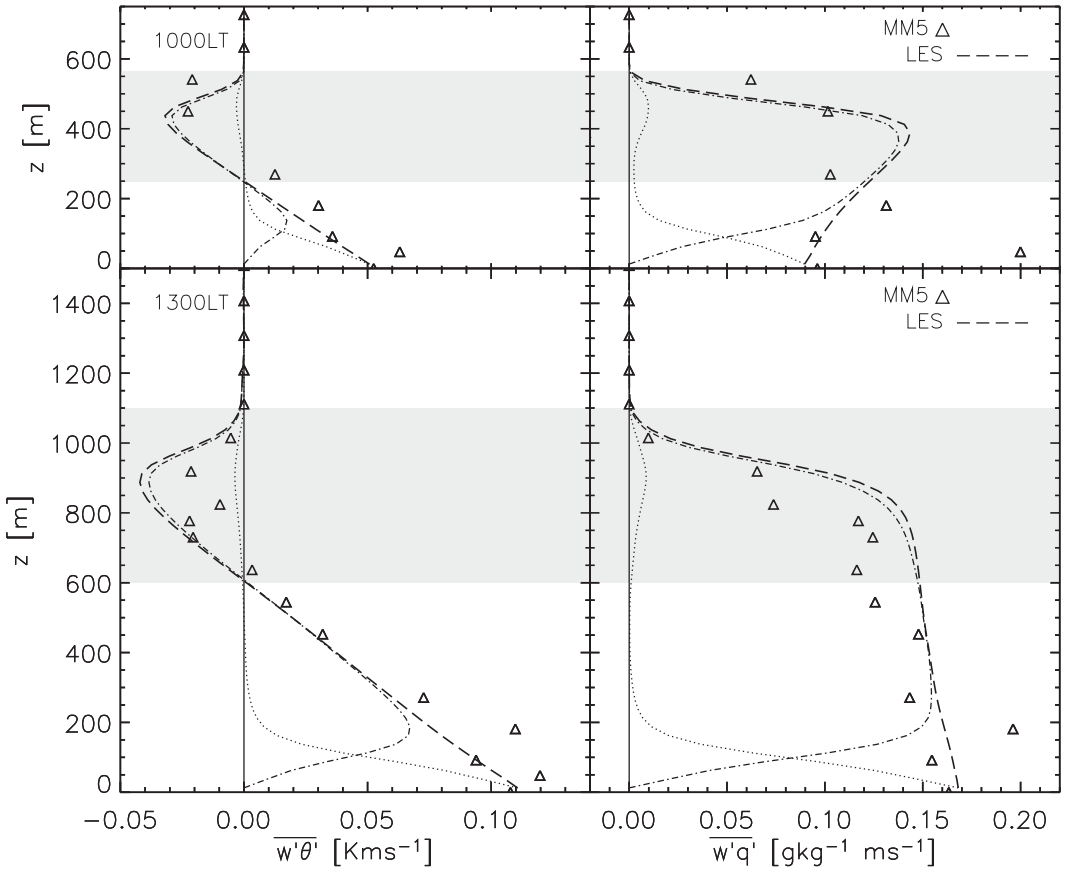

FIG. 4. The turbulent flux profile of (left) potential temperature and (right) specific humidity at (top) 1000 LT and (bottom) 1300 LT from MM5 (triangles; averaged over the fourth domain) and DALES (black dashed line; averaged over a 25.6 × 25.6 km^2 domain), including the resolved (dashed–dotted line) and subgrid (dotted line) contribution.

analyzed the idealized heterogeneous experiment of MM5 and DALES.

Figure 6 shows the west–east cross sections for potential temperature and vertical wind speed for MM5 (Fig. 6a) and DALES (Fig. 6b) and for specific humidity and horizontal wind speed (MM5: Fig. 6c; DALES: Fig. 6d). In DALES the horizontal variables were averaged over 1 km (10 grid points) to allow identical horizontal resolution of the output of the two models. Furthermore, for MM5 the instantaneous output at 1300 LT was used, whereas output from DALES was averaged over 15 min. Notice that we used a different criterion to estimate the boundary layer height in DALES here, because above the cold patch a sharp gradient at the inversion of θ_v did not exist. Here, h is the level at which TKE is 10% of its maximum.

Both models identified a higher θ and a deeper boundary layer above the west patch (warm and dry) driven by the larger sensible heat flux. They also reproduced rising air above the warm patch (west) and descending air above the cold patch (east) (Figs. 6a,b). Close to the surface, cold moist air was transported from east to west, and just below h warm air was advected from west to east (Figs. 6c,d). In other words, a mesoscale circulation cell was reproduced in both models, as was also simulated by Avissar and Schmidt (1998) and Patton et al. (2005) using LES techniques. Some essential differences were found between MM5 and DALES, however. In DALES, we found a strong narrow updraft (the maximum vertical wind speed w was 0.81 m s^{-1}) and a weak sinking motion ($w = -0.25$ m s^{-1}) over a large area (Fig. 6b). These observations are comparable to those of Avissar and Schmidt (1998) and Patton et al. (2005), whereas in MM5 the updraft was smaller by a factor of almost 6 than in DALES ($w = 0.13$ m s^{-1}). Moreover, in MM5 the updraft was only 2 times as strong as the downdraft ($w = -0.08$ m s^{-1}), and it covered the entire west patch (Fig. 6a). The horizontal wind in DALES was also larger in the lower and upper part of the cell: $U_{\mathrm{DALES}} = -2.9$ m s^{-1} and $U_{\mathrm{MM5}} = -1.3$ m s^{-1} at the surface, and $U_{\mathrm{DALES}} = 2.9$ m s^{-1} and $U_{\mathrm{MM5}} = -1.9$ m s^{-1} below the top of the boundary layer. As a result of the small updraft area in DALES, $U_{\max}$ was located farther

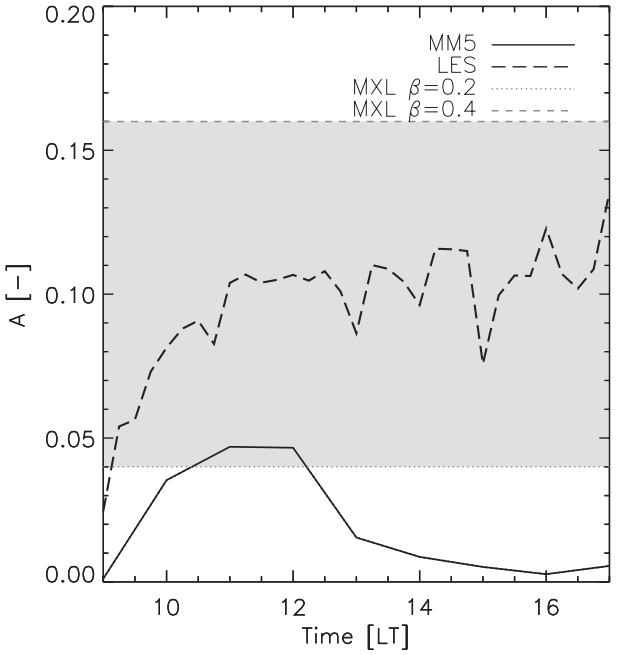

FIG. 5. Time evolution of the ratio A between the integral of the negative parts N and the positive parts P of the virtual potential temperature flux from MM5 (solid line) and DALES (dashed line).

to the west in DALES ($x/\lambda = -0.1$ for DALES and $x/\lambda = 0$ for MM5). To summarize, the circulation is more intense and more centered above the warm patch surface in DALES than in MM5.

Below we suggest that the differences in reproducing the circulation between MM5 and DALES were due in the first place to the explicit (DALES) or parameterized (MM5) solution of turbulent motion and second to the interactions of the mesoscale cell with the boundary layer dynamics. As explained by van Heerwaarden and Vilà-Guerau de Arellano (2008), a consequence of the surface heterogeneity in DALES is that upward thermals were concentrated over the warm patch. Above the cold patch the upward thermals were suppressed, because of the downward motion of the mesoscale cells, and did not even reach h, as shown in Fig. 6. In other words, in DALES, surface heterogeneity largely changed the turbulent pattern with respect to homogeneous conditions. On the other hand, in MM5, upward thermals cannot be congregated above the warm patch and suppressed above the cold patch, because of the imposed parameterization of turbulence [Eqs. (1) and (2)]. MM5 thus represented the vertical turbulent structure in the heterogeneous case in a way that is more similar to the homogeneous case. As Fig. 6 shows, MM5 still reproduced a well-mixed boundary layer, whereas DALES showed a gradient for θ and q in a large part of the upper branch of the boundary layer in the east (cold and wet). For instance, the potential temperature was well mixed up to a level of approximately 600 m in MM5 (Fig. 6a), whereas in DALES the mixing of θ in the upper part of the boundary layer was stagnant, especially at $x/\lambda = 0.25$, where the downward motion of the mesoscale circulation was at a maximum (Fig. 6b). The specific humidity also displayed a relatively well-mixed boundary layer in MM5, whereas the specific humidity field in DALES showed a large dry intrusion (cf. Figs. 6c,d).

As a consequence, when turbulence was parameterized in a mesoscale model, a decoupling of the turbulent movement and larger-scale motion was found. As a result, in MM5, the effect of turbulence in the flow was less suppressed and the boundary layer was still relatively well mixed above the cold patch, and the mesoscale circulation was weaker.

The different treatment in the circulation cell had a direct effect on the boundary layer dynamics. First, in DALES the boundary layer height showed a steep peak in the west ($x/\lambda = -0.25$) and a deep trough in the east ($x/\lambda = 0.25$), at the same location as the maximum and minimum values of w at 1300 LT (Fig. 6). The specific humidity pattern also differed. The q maximum at the surface was located farther to the west by DALES, even above the dry surface patch ($x/\lambda = -0.15$ and $x/\lambda = -0.35$), indicating that close to the surface more moist air was being transported from east to west. Note that for DALES two q maxima were visible, whereas MM5 located only one q maximum at $x/\lambda = 0$ rather than at the westerly border of the domain. This is a result of the cyclic boundary conditions in DALES as compared with the small soil moisture difference with respect to the larger domain and the west patch (M is respectively 50% and 30%) in MM5.

2) THERMODYNAMICS

In this section, we further quantify the influence of different representations of the mesoscale circulation on the heat and moisture budgets under conditions of surface heterogeneity. The bulk potential temperature $\langle\theta\rangle$ and bulk specific humidity $\langle q\rangle$ were therefore calculated by horizontally and vertically averaging θ and q over the entire boundary layer. Figure 7 shows the temporal evolution of the bulk values for MM5 and DALES, averaged both over the entire heterogeneous area and over the two patches separately.

The differences in $\langle\theta\rangle$ between the west and east patch were expected. Both models identified a higher temperature above the west patch than above the east patch, due to the higher sensible heat flux. W can, however, see interesting differences between the models. DALES found an initial larger $\langle\theta\rangle$ than did MM5, whereas in the homogeneous case they agreed (Fig. 2). The reason for this is that h calculated with the TKE method is a bit

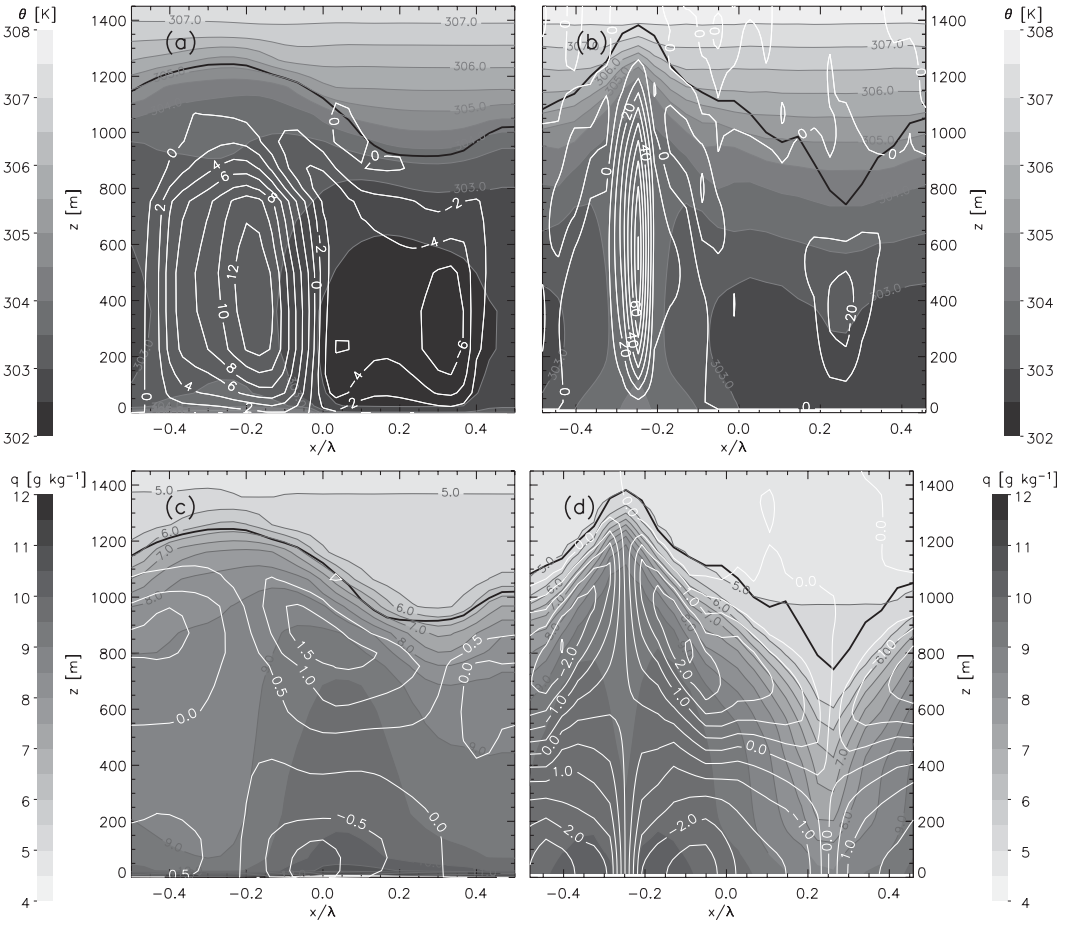

FIG. 6. The averaged west–east cross section of (a), (b) potential temperature (shaded) and vertical wind speed (cm s^{-1}; white contours) and (c), (d) specific humidity (shaded) and horizontal wind speed (m s^{-1}; white contours) for (left) MM5 and (right) DALES observed above the heterogeneous cases at 1300 LT. The thick black line represents the boundary layer height. Note that DALES was horizontally averaged over 1 km to ensure comparable horizontal resolution.

larger than that calculated with the maximum gradient method. Furthermore, in DALES the bulk temperatures of the two patches converged (especially after 1300 LT) whereas in MM5 the difference between the patches remained the same. Because of the strong circulation in DALES, warm air entrained above the west patch was horizontally advected to the east (see Fig. 6). Analysis of cross sections for later that day (e.g., at 1500 LT; figure not shown) revealed that the warm air that was transported from west to east at the top of the boundary layer even reached the surface of the east cold patch, where it was directly advected to the west again. In other words, in DALES after 1300 LT, the influence of the mesoscale circulation on the temperature becomes stronger, which caused the bulk temperature to be better transported horizontally.

The contrast in $\langle q \rangle$ between the west and east patches of the heterogeneous case confirmed the role of the induced circulation. Because of the higher surface $L_v E$ over the east in both models, $\langle q \rangle$ was larger there at the beginning of the day until 1000 LT for DALES and until 1400 LT for MM5. After these times, the moister air was found above the originally dry patch. This was caused by the mesoscale circulation: moist air was transported from east to west at the surface and dry air, entrained above the west patch, was advected to the east at the top of the boundary layer. The 4-h delay in the transport of the moist air in MM5, relative to that in DALES, was due to a much weaker circulation in MM5. We also observed in DALES that after 1300 LT $\langle q \rangle_{\text{east}}$ increased and $\langle q \rangle_{\text{west}}$ decreased slightly. From the afternoon cross sections (not shown) we found that humid air, which entered the boundary layer above the wet patch near the surface, was vertically transported to higher levels. Dry air that entered above the cold and wet east patch was transported downward to the surface and advected over

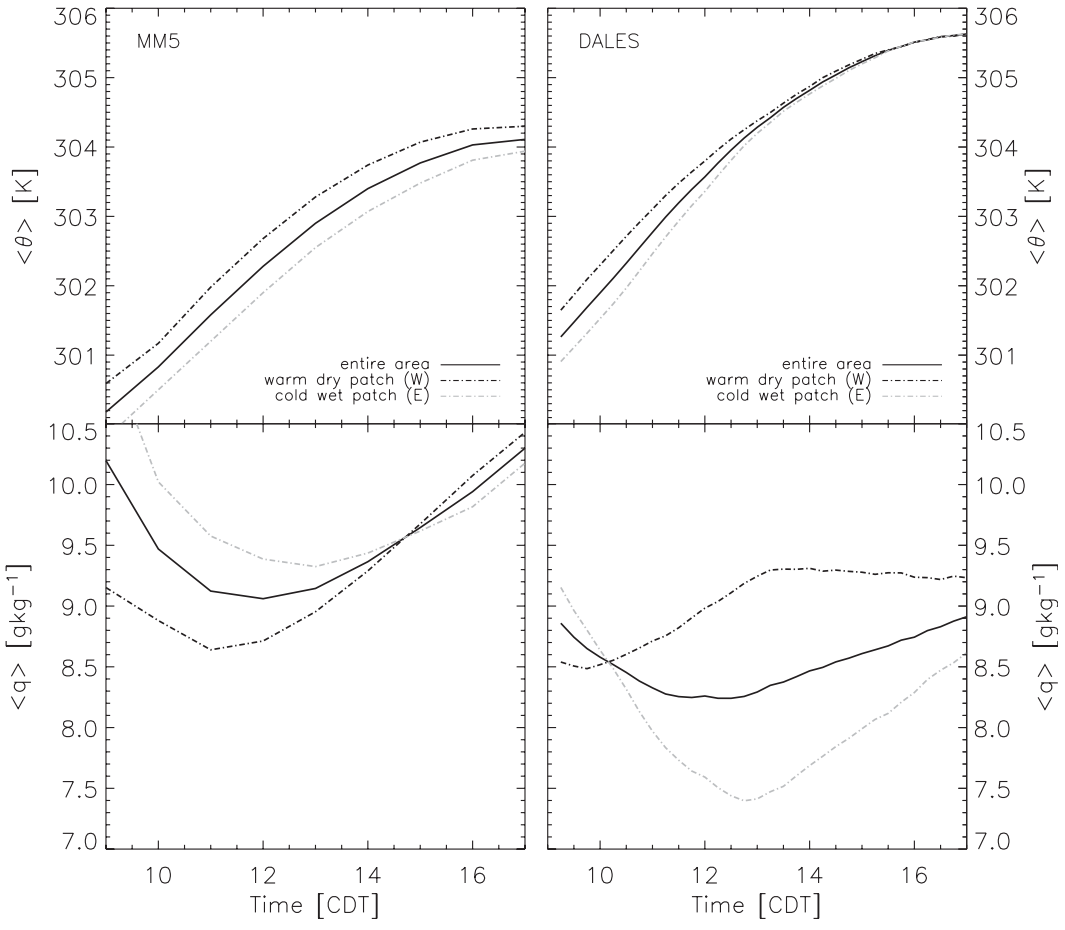

FIG. 7. Temporal evolution of the mixed layer (top) potential temperature and (bottom) specific humidity from (left) MM5 and (right) DALES. These are the averaged values over the entire heterogeneous domain (solid line) and averaged values of the west patch (dark-gray dashed–dotted line) and east patch (light-gray dashed–dotted line).

the west patch. In sum, later in the day, the influences of the strong circulation in DALES yielded a better mixing of specific humidity, similar to potential temperature.

c. *Land–atmosphere coupling in MM5*

The previous section showed that the turbulent parameterization scheme resulted in a weak circulation in MM5 above the heterogeneous surface. As mentioned in section 2a, the boundary layer scheme is coupled with a land surface scheme in MM5. It would thus be interesting to investigate the influences of the horizontal variability in soil moisture and the mesoscale circulation on the surface fluxes, comparing the heterogeneous and homogeneous cases. In this section, we quantify the response of the land–atmosphere coupling to modifications of M in MM5.

In addition to studying the effects of the mesoscale circulation on land–atmosphere coupling, it is worth analyzing the response of M modifications in MM5. We therefore performed two additional homogeneous MM5 experiments. The first was a simulation under dry conditions ($M = 30\%$) comparable to the west patch of the heterogeneous run, and the second had soil moisture of 70%, similar to the east patch.

Table 6 shows horizontally averaged H and L_vE at 1300 LT for all of the experiments. According to the surface flux parameterization [Eq. (4)], M is linearly related to L_vE, which was not found in the results. In the three homogeneous experiments, we observed a decrease in L_vE of 21% when M was 40% lower (from 50% to 30%), and an M increase of 40% (from 50% to 70%) resulted in a 12% increase of L_vE (Table 6). The nonlinear response was observed because variations in L_vE will change several other atmospheric variables (e.g., sensible heat flux, air temperature, boundary layer depth, and entrainment), which in turn again affects L_vE. This was caused by a number of positive and negative feedbacks in the atmosphere and between land and atmosphere, as illustrated, for example, in Fig. 1 from Ek and Mahrt (1994) and Fig. 1 from van Heerwaarden

TABLE 6. Horizontally averaged surface fluxes of the three homogeneous MM5 experiments at 1300 LT.

	M (%)	Sensible heat flux (W m^{-2})	Latent heat flux (W m^{-2})
Original homogeneous	50	126	474
Dry homogeneous	30 (−40%)	198 (+57%)	376 (−21%)
Wet homogeneous	70 (+40%)	84 (−33%)	533 (+12%)
Heterogeneous	30 (west) and 70 (east)	141	457
Heterogeneous west patch	30	225	356
Heterogeneous east patch	70	64	551

et al. (2009). Comparing the horizontal averaged fluxes of the heterogeneous experiment with the original homogeneous experiment, we observed that H was 16 W m^{-2} higher and L_vE was 17 W m^{-2} lower for the heterogeneous run. As a consequence, the total amount of energy available for the turbulent fluxes was comparable in both experiments: approximately 600 W m^{-2}.

To discuss the effect of surface heterogeneity on surface fluxes, we show how the fluxes varied along the surface heterogeneity. Figure 8 presents H and L_vE from west to east for the four runs at 1300 LT. As expected, the fluxes differed between west and east in the heterogeneous case. The transition of H and L_vE between west and east was not gradual; H had higher (lower) values in the eastern (western) part of the dry (wet) patch than in the center of this patch.

Two reasons for the nongradual transition are suggested. First, as explained by Patton et al. (2005), because of the induced circulation, stagnation in the horizontal wind speed was found over the center of the dry patch (see at $\lambda = -0.25$ in Fig. 6b), producing the lower values for the fluxes there [see Eqs. (3) and (4)]. Second, because of the M difference between west and east, the surface temperature T_s displayed a sharp transition between the two patches; T_s varied by 3 K between west and east, and the transition zone was 1 km wide (one grid box). The advection of cold air from east to west lowered the surface air temperature T_a above the west patch. As a result, the transition of T_a was more gradual and smoother: the first-layer temperature varied by 1.5 K over a width of almost 5 km. The temperature difference $T_s - T_a$ had a maximum value at the eastern boundary of the west patch and a minimum value at the western boundary of the east patch (between $\lambda = -0.05$ and 0.01). Since the temperature difference shows the largest differences between the two patches, it results in a nongradual transition of H [Eq. (3)]. Because of the moist air advection from the wet east patch over the dry west patch, q_a displayed a more gradual transition than q_s. As a result, $q_a - q_s$ and therefore L_vE were not gradual [Eq. (4)]: the maximum was located near the western part of the wet patch, and the minimum was located toward the eastern part of the dry patch.

Two questions remain unanswered: 1) How much were H and L_vE driven by the interaction of the induced mesoscale circulation with the surface processes? 2) Are the induced H and L_vE modifications by surface heterogeneity a positive or negative feedback on the mesoscale circulation? The gray shaded areas in Fig. 8 indicate the increases or decreases in value of the surface fluxes over the west dry and east moist patch of the heterogeneous case with respect to the homogeneous dry and moist experiments. In other words, the areas represent the surface flux modifications caused by the interaction of the induced mesoscale circulation with the surface. The advection of cold moist air at the surface induced by the surface heterogeneity led to a fall in T_a and a rise in q_a above the west patch (see Fig. 6). As a result, $T_s - T_a$ and therefore H [Eq. (3)] were larger over the west patch than above the dry homogeneous case, whereas $q_a - q_s$ and consequently L_vE [Eq. (4)] became smaller above the west patch. The effect of the cold-air advection on H was an increase of 27 W m^{-2}, from an average value of 198 W m^{-2} in the homogeneous dry case to an average value of 225 W m^{-2} over the west dry patch in the heterogeneous case (Table 6). For L_vE the effect is smaller: −20 W m^{-2}. In the east the opposite effect was observed: as a consequence of the transport of warm, dry air near h, T_a increased and q_a decreased. This led to smaller $T_s - T_a$ (higher $q_a - q_s$) and subsequently to a lower H (larger L_vE) over the east patch in the heterogeneous case than over the homogeneous wet case. The above-mentioned process describes a positive feedback: the surface heterogeneity led to the development of a mesoscale circulation, which in turn strengthened the surface flux heterogeneity. It is not sufficient to model the more powerful circulation as obtained by DALES, however.

4. Conclusions

To study the boundary layer parameterization scheme (MRF) in MM5 with DALES under homogeneous and heterogeneous conditions, we have taken a multiple single-column modeling approach. This approach implies that the mesoscale model is initialized and updated with

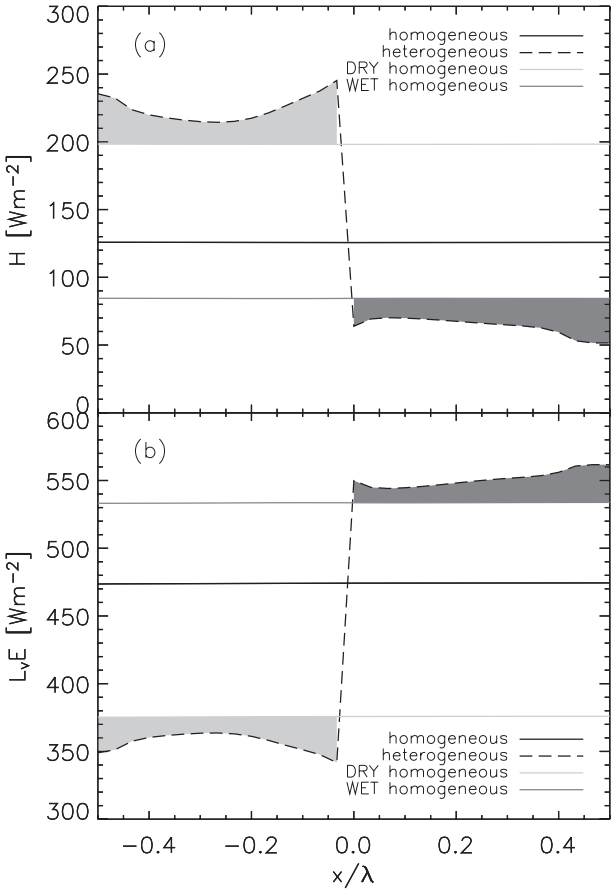

FIG. 8. The surface (a) sensible and (b) latent heat fluxes from west to east at 1300 LT, for the standard homogeneous case (black solid line), the dry homogeneous case (light-gray dash–dotted line), the wet homogeneous case (dark-gray dash–dotted line), and the heterogeneous case (black dashed line) of MM5. The values were averaged along the north–south direction. The shaded regions indicate the increase or decrease in the amount of energy that entered the boundary layer over the wet or dry patch in the heterogeneous case, relative to the homogeneous dry and wet cases.

idealized surface and upper-air conditions for every grid box to perform numerical control experiments using the mesoscale and LES models. We designed two experiments using the MSC approach. In the first experiment (homogeneous), we prescribed uniform surface conditions. The second experiment (heterogeneous) had differences in soil moisture between the west (M = 30%) and east (M = 70%) in MM5 and a surface flux variability for DALES. The low relative standard deviation (of, e.g., H, L_vE, and h) observed from the homogeneous run indicated that MM5 acts as an MSC technique. This enabled us to use the MM5 results to validate the MRF parameterization scheme with DALES.

From the homogeneous case we observed that the boundary layer dynamics were comparable for the two models. The MRF boundary layer scheme underestimated turbulent mixing near the surface and entrainment of warmer and drier air, however. Because of the inefficient turbulence near the surface, steep gradients of potential temperature and specific humidity were found. In combination with the use of the nonlocal mixing scheme in MRF, a parcel could move to higher levels, which resulted in a deeper boundary layer for MM5 in the morning. During the day entrainment was underestimated by MM5; we therefore observed a colder and moister boundary layer during the day and a shallower boundary layer in the afternoon when compared with DALES. Moreover, despite the underestimation in the entrainment zone, the turbulent flux profile showed a comparable pattern under the two models.

Above a heterogeneous surface, both models reproduced a mesoscale circulation with updrafts above the warm and dry patch and downward transport above the cold and wet patch. However, we found differences in the circulation characteristics of the two models. In DALES, surface heterogeneity influenced the turbulent pattern, whereas in MM5 this cannot occur because of the imposed parameterization of turbulence. The MRF parameterization scheme underestimated the circulation ($w_{\max}$ is smaller by a factor of 6), and above the cold patch MM5 showed still a relatively well mixed boundary layer for θ and q. As a consequence, the boundary layer dynamics between the two models differ more over a heterogeneous surface than over a homogeneous area.

Because of the stronger circulation in DALES, several other boundary layer quantities differed between MM5 and DALES. For instance, h had a steep peak and deep trough in DALES. Furthermore, during the day the bulk temperatures averaged above the patches converged in DALES, whereas in MM5 the difference between the potential temperatures above the two patches remained the same. Moreover, in DALES the highest values of the bulk specific humidity above the surface wet patch (east) were found 4 h earlier with respect to MM5, because of more advection of dry air from west to east at the top of the boundary layer and moist air from east to west near the surface.

As a consequence of the land–atmosphere coupling in MM5, advection of cold moist air at the surface induced by the surface heterogeneity led to a fall in air temperature and a rise in specific humidity near the surface above the warm patch. As a result, the temperature (humidity) difference and therefore the sensible (latent) heat flux increased (decreased). In other words, surface heterogeneity produced a mesoscale circulation, which in turn strengthened the surface heterogeneity in MM5.

This study shows that the MSC approach is an appropriate method of evaluating and studying the turbulent scheme in a mesoscale model with a large-eddy

simulation model, for example, to determine the ability to represent entrainment processes and a mesoscale circulation. In particular, surface heterogeneity can also be investigated with the MSC approach, unlike with a single-column model. From our study we conclude that it is important to further compare DALES and MM5 by means of control experiments above heterogeneous surfaces, because the boundary layer characteristics modeled by the two models differed more above a heterogeneous surface than above a homogeneous surface, because of the decoupling between turbulent transport and larger-scale motions in the mesoscale model. Furthermore (not discussed in this study), we expect that the MSC approach could also be an optimal tool for sensitivity studies of different physical parameterization schemes or of various parameters within the same scheme.

Acknowledgments. We thank Chiel van Heerwaarden (Wageningen University) for useful discussions and valuable comments. The large-eddy simulations in this research were performed at SARA Computing and Networking Services and were financially supported by the National Computing Facility Foundation (NCF SH-060-10). We appreciate the anonymous reviewers and the editor giving critical remarks and suggestions that helped to improve the manuscript.

REFERENCES

Avissar, R., and T. Schmidt, 1998: An evaluation of the scale at which ground surface heat flux patchiness affects the convective boundary layer using large eddy simulation. *J. Atmos. Sci.,* **55,** 2666–2689.

Ek, M., and L. Mahrt, 1994: Daytime evolution of relative humidity at the boundary layer top. *Mon. Wea. Rev.,* **122,** 2709–2721.

Górska, M., J. Vilà-Guerau de Arellano, M. A. LeMone, and C. C. van Heerwaarden, 2008: Mean and flux horizontal variability of virtual potential temperature, moisture, and carbon dioxide: Aircraft observations and LES study. *Mon. Wea. Rev.,* **136,** 4435–4451.

Grell, M. B., J. Dudhia, and D. R. Stauffer, 1994: A description of the fifth generation Penn State/NCAR Mesoscale Model (MM5). NCAR Tech. Note NCAR/TN 397+IA, 114 pp.

Heus, T., and Coauthors, 2010: Formulation and numerical studies with the Dutch Atmospheric Large-Eddy Simulation (DALES). *Geosci. Model Dev. Discuss.,* **3,** 99–180.

Holtslag, A. A. M., and B. A. Boville, 1993: Local versus nonlocal boundary layer diffusion in a global climate model. *J. Climate,* **6,** 1825–1842.

——, E. van Meijgaard, and W. C. De Rooy, 1995: A comparison of boundary layer diffusion schemes in unstable conditions over land. *Bound.-Layer Meteor.,* **76,** 69–95.

Hong, S. Y., and H. L. Pan, 1996: Nocturnal boundary layer vertical diffusion in a medium range forecast model. *Mon. Wea. Rev.,* **124,** 2322–2339.

LeMone, M. A., F. Chen, J. G. Alfieri, M. Tewari, B. Geerts, W. Miao, R. Grossman, and R. Coulter, 2007: Influence of land cover, soil moisture, and terrain on the horizontal distribution of sensible and latent heat fluxes and boundary layer structure in southeast Kansas during IHOP2002 and CASES 97. *J. Hydrometeor.,* **8,** 68–87.

Lenderink, G., and Coauthors, 2004: The diurnal cycle of shallow cumulus clouds over land: A single-column model intercomparison study. *Quart. J. Roy. Meteor. Soc.,* **130,** 3339–3364.

Letzel, M. O., and M. O. Raasch, 2003: Large-eddy simulation of thermally induced oscillations in the convective boundary layer. *J. Atmos. Sci.,* **60,** 2328–2341.

Mahrt, L., 2000: Surface heterogeneity and vertical structure of the boundary layer. *Bound.-Layer Meteor.,* **96,** 33–62.

Patton, E. G., P. P. Sullivan, and C. H. Moeng, 2005: The influence of idealized heterogeneity on wet and dry planetary boundary layers coupled to the land surface. *J. Atmos. Sci.,* **62,** 2078–2097.

Pino, D., J. Vilà-Guerau de Arellano, and S. Kim, 2006: Representing sheared convective boundary layer by zeroth- and first-order-jump mixed-layer models: Large-eddy simulation verification. *J. Appl. Meteor. Climatol.,* **45,** 1224–1243.

Steeneveld, G. J., T. Mauritsen, E. I. F. de Bruijn, J. Vilà-Guerau de Arellano, G. Svenson, and A. A. M. Holtslag, 2008: Evaluation of limited area models for the representation of the diurnal cycle and contrasting nights in CASES-99. *J. Appl. Meteor. Climatol.,* **47,** 869–887.

Sullivan, P. P., C. Moeng, B. Stevens, D. H. Lenschow, and S. D. Mayor, 1998: Structure of the entrainment zone capping the convective atmospheric boundary layer. *J. Atmos. Sci.,* **55,** 3042–3064.

Tennekes, H., 1973: A model for the dynamics of the inversion above a convective boundary layer. *J. Atmos. Sci.,* **30,** 558–567.

——, and A. G. M. Driedonks, 1981: Basic entrainment equations for the atmospheric boundary layer. *Bound.-Layer Meteor.,* **20,** 515–531.

Troen, I. B., and L. Mahrt, 1986: A simple model of the atmospheric boundary layer; sensitivity to surface evaporation. *Bound.-Layer Meteor.,* **37,** 129–148.

van Heerwaarden, C. C., and J. Vilà-Guerau de Arellano, 2008: Relative humidity as an indicator for cloud formation over heterogeneous land surfaces. *J. Atmos. Sci.,* **65,** 3263–3277.

——, ——, A. F. Moene, and A. A. M. Holtslag, 2009: Interactions between dry-air entrainment, surface evaporation and convective boundary-layer development. *Quart. J. Roy. Meteor. Soc.,* **135,** 1277–1291.

Vilà-Guerau de Arellano, J., O. S. Vellinga, A. A. M. Holtslag, F. C. Bosveld, and H. Klein Baltink, 2001: Observational evaluation of PBL parameterizations modelled by MM5. Preprints, *11th PSU/NCAR MM5 User Workshop,* Boulder, CO, National Center for Atmospheric Research, 102–105. [Available online at http://www.mmm.ucar.edu/mm5/workshop/ws01/vila.pdf.]

Weckwerth, T., and Coauthors, 2004: An overview of the International H_2O Project (IHOP_2002) and some preliminary highlights. *Bull. Amer. Meteor. Soc.,* **85,** 253–277.

Zhong, S., and J. Fast, 2003: An evaluation of the MM5, RAMS, and Meso-Eta models at subkilometer resolution using VTMX field campaign data in the Salt Lake Valley. *Mon. Wea. Rev.,* **131,** 1301–1322.

——, H. In, and C. Clements, 2007: Impact of turbulence, land surface, and radiation parameterizations on simulated boundary layer properties in a coastal environment. *J. Geophys. Res.,* **112,** D13110, doi:doi:10.1029/2006JD008274.